

# Chapter 14

## Structural Optimization of 3D Wings Under Aerodynamic Loads: Topology and Shell

Volker Schulz, Roland Stoffel and Heinz Zorn

**Abstract** New methods in manufacturing and novel challenges and usages require the exploration of the potential of new wing designs. This is the goal of this paper. We propose novel computational methods for the robust optimization of wings under aerodynamic loads. We restrict the discussion to the optimization of the linear-elastic properties of wings concerning several load cases and with treatment on deformations and regularization. The degrees of freedom for the design itself are the interior structure of the wing leading to topology optimization aspects and the structure of the wing hull in terms of composite material. Thus, this paper aims at mathematical methods for topology optimization of the wing interior made of isotropic material, the optimization of orthotropic composite material in the wing hull and the proper treatment of practical deformation aspects and multiple loads in this context.

### 14.1 Introduction

We develop mathematical methods for wings with the abstract coarse structure in Fig. 14.1. The 3D wing consist of two major parts, the interior (light grey), which we denote as  $\Omega_0$  and the wing hull (dark grey), which we denote as  $\Omega_1$ .

We aim at the minimization of the elastic compliance, i.e., the computational treatment of the following optimization problem with constraints in the form of the elasticity equation:

$$\begin{aligned} \min W_{\Omega} &:= \int_{\Omega} \sigma(u) : \varepsilon(u) dx \\ \text{subject to} \quad & -\operatorname{div}(\sigma(u)) = 0 \text{ in } \Omega := \Omega_0 \cup \Omega_1 \end{aligned}$$

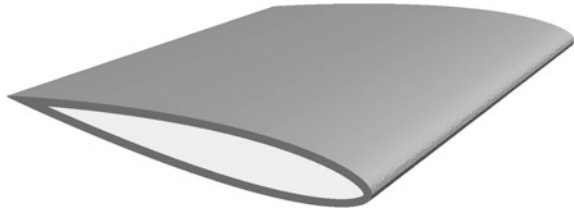
---

V. Schulz (✉)

Steinbeis-Innovationszentrum Modellbasierte Mathematische Optimierung,  
Januaris-Zick-Str. 73, 54296 Trier, Germany  
e-mail: volker.schulz@uni-trier.de

R. Stoffel · H. Zorn  
Trier University, Trier, Germany

**Fig. 14.1** Exemplaric NACA wing illustrating the coarse structures treated in this paper



$$\begin{aligned} \sigma(u) &= C\varepsilon(u) \text{ in } \Omega \\ u &= 0 \text{ on } \Gamma_{\text{fix}} \\ \sigma(u)n &= g \text{ on } \Gamma_{\text{force}} \end{aligned}$$

where  $\Gamma_{\text{fix}} \cup \Gamma_{\text{force}} = \partial\Omega$

Here,  $u : \Omega \rightarrow \mathbb{R}^3$  denotes the deformation vector field and  $\varepsilon, \sigma$  the strain and stress tensors, furthermore  $C : \Omega \rightarrow \mathbb{R}^{3 \times 3 \times 3 \times 3}$  the spatially varying stiffness matrix. The boundary  $\Gamma_{\text{fix}}$  is the part of the wing boundary, where the wing is attached to the body of the aircraft, and the boundary  $\Gamma_{\text{force}}$  is the part, which the aerodynamic loads  $g : \Gamma_{\text{force}} \rightarrow \mathbb{R}^3$  are acting on. The degree of freedom for optimization is the stiffness matrix, where we—in contrast to free material optimization [1]—do not admit an arbitrary structure. In the interior  $\Omega_0$ , we rather assume that the stiffness matrix is a scalar multiple of an isotropic tensor, i.e.,  $C_0 = \rho E_0$ , where  $\rho : \Omega_0 \rightarrow \mathbb{R}$  and  $E_0$  is constant. Furthermore, we assume that the stiffness matrix in the hull,  $\Omega_1$ , depends locally and orthotropically on the local fiber orientation, i.e.,  $C_1 = C_1(\alpha)$ , where  $\alpha : \Omega \rightarrow \mathbb{R}$ . The subsequent sections focus on  $\Omega_0, \Omega_1$  and practical aspects.

## 14.2 Topology Optimization of the Wing Interior

Topology optimization aims at optimal structures or—more precisely—optimal material distributions in the subdomain  $\Omega_0 \subset \Omega \subset \mathbb{R}^3$  with respect to minimization of elastic energy (compliance). The amount of material is not allowed to surpass a certain maximal volume, i.e.,  $\int_{\Omega_0} dx \leq V$ . A decisive aspect is the representation of the boundary  $\Gamma = \partial\Omega_0$ , for which the level set method of Osher/Fedkiew [2] or Sethian [3] is a powerful tool. Several approaches exist to topology optimization:

- SIMP method
- shape optimization based on the shape calculus
- topology optimization based on the topological calculus

The *SIMP* (solid isotropic material with penalization) method of Bendsoe and Sigmund [4] uses a homogenization approach to structural optimization. They introduce a pseudo density function  $\rho \in \{0, 1\}$ . If the density at a point (or in an element of the discretization mesh) is 0, there does not exist any material. If it is 1,

then there exists material there. Based on this interpretation of material structure, gradient based algorithms are used in order to compute a locally optimal density distribution  $\rho$ . Additional difficulties resulting from relaxation ( $\rho(x) \in (0, 1)$ ) and potential checkerboarding have to be treated, e.g., by filtering techniques (cf., [4, 5]). However, those techniques are hardly computationally viable on unstructured grids.

Shape optimization based on the shape calculus is used in several industrial applications. The theoretical foundations can be found in [6, 7]. Optimal shapes for fluid flow is considered, e.g., in [8] and also [9–11]. If shape optimization is used for the purpose of topology optimization as in [12], it is assumed that there are already holes (regions without material) in the domain. The aim is to compute the optimal shapes of the boundaries of those holes. The shape calculus is used to compute shape sensitivities on the boundaries. The resulting shape gradient guides the computation towards a (local) optimum. The method uses an explicit representation of the boundaries. A severe drawback is that the number of holes cannot be changed by this approach. This problem can be circumvented by a combination of shape optimization with a level set method. The level set method describes the boundaries of the holes as contour surface (usually the zero contour surface) of a higher dimensional level set function  $\Phi$ . The evolution of the boundaries is described by the so called level set equation, which is a time dependent convection equation. In this way, holes are enabled to merge. However, this method does not possess a mechanism to create new holes. Good computational performance is achieved for level set functions in the form of signed distance functions, which require frequent re-initialization during the optimization process. Furthermore, the shape gradient, which exists only on the contour surface, has to be somehow propagated on the whole computational domain.

The creation of new holes is enabled by the usage of the so-called topological derivative, which has been introduced by Sokolowski and Zochowski [13] in 1999. The concept of topological derivative is frequently used in image processing and inverse modeling.

The topological derivative compares function evaluations on shapes without a hole and with a small hole in the form of a difference quotient. Thus, it is the limit of the difference quotient and can be related to shape gradients. In this particular case, the topological derivative of the compliance in 3D at the position  $x \in \Omega_0$  can be expressed as (cf. [14, 15])

$$D_T W_{\Omega}(x) = \frac{3}{4} \frac{1-\nu}{7-5\nu} \left[ 10\sigma(u) : \varepsilon(u) - \frac{1-5\nu}{1-2\nu} \text{tr}\sigma(u)\text{tr}\varepsilon(u) \right] (x).$$

where  $\nu$  is the Poisson ratio of the material. A rather elegant method for structural optimization is the combination of the topological derivative with the level set method as described in [16]. In this approach, the domain  $\Omega_0$  is divided in one region with material  $\{x \mid \Phi(x) \leq 0\}$  and another region without material  $\{x \mid \Phi(x) > 0\}$ . The topological derivative is used as an indicator, where material should be added or reduced. A local optimum is reached at a fixed point of this strategy, as soon as the sign of the topological derivative coincides with the sign of the level set function everywhere.

The publication [17] discusses a topological sensitivity analysis for linear elasticity in 2D without level set function approach. The sensitivity analysis in 3D is carried out in [14], again without a level set framework. The level set method of Amstutz with inclusions is described in [16], referencing [18] for the sensitivity analysis. [19] introduces the level set framework together with a penalization of constraints. In [20], augmented Lagrangian approaches for the proper treatment of constraints within a topology optimization context are investigated but in the context of linear elasticity.

The topology optimization approach proposed in this paper consists of the following components:

- discretization and solution of the elasticity equations by usage of the open source software toolbox FEniCS [21].
- 3D implementation of the topological gradient described in [14] for the linear elasticity solver FEniCS in combination with the
- level set approach in [16, 19].
- Furthermore, it is necessary to limit the volume of the optimal structures. For the treatment of additional constraints of this type, we use an augmented Lagrangian technique as described in [16, 19].

In the sequel, we describe numerical results of this strategy for the following testcase: we use a wing in the shape of a NACA prism as in Fig. 14.1. This wing is exposed to a usual pressure profile, which is constant in longitudinal direction. The elasticity equation is discretized in the wing interior on 8 million tetraedral elements with 1.5 million nodes and with linear finite elements. From that result 4.6 million unknowns, for which the discretized elasticity equations are solved on a parallel computing architecture in each optimization iteration. The optimization needs 180 iterations according the optimization approach discussed above. For the interior wing structures, we allow only 10% of the maximum possible material volume, i.e.,  $V_0 = 0.1 \cdot |\Omega_0|$ . Figures 14.2 and 14.3 show the achieved solution from different perspectives. We note that the results of this test case can be geometrically interpreted as longitudinally curved truss-like structures, which challenge the usually used rib structures.

Similar investigations can be performed with wings with a priori rib structures in the interior as in Fig. 14.4.

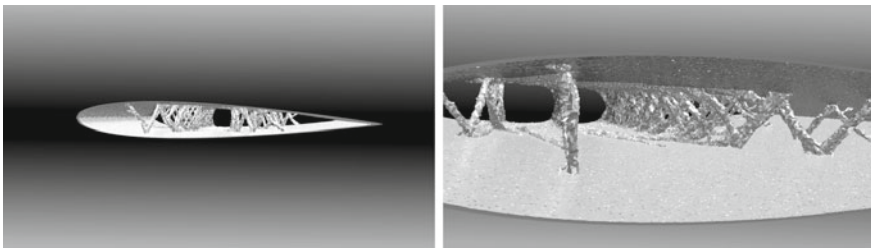


**Fig. 14.2** View into the optimized wing tip (left) and in detail (right)

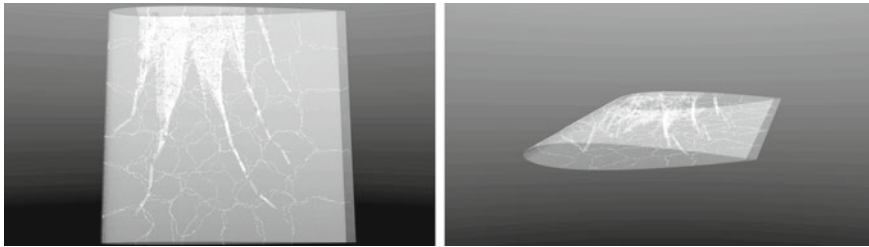


**Fig. 14.3** Transparent rendering of the optimal wing from different angles. The thin net-like structures show the domain decomposition for parallel computing

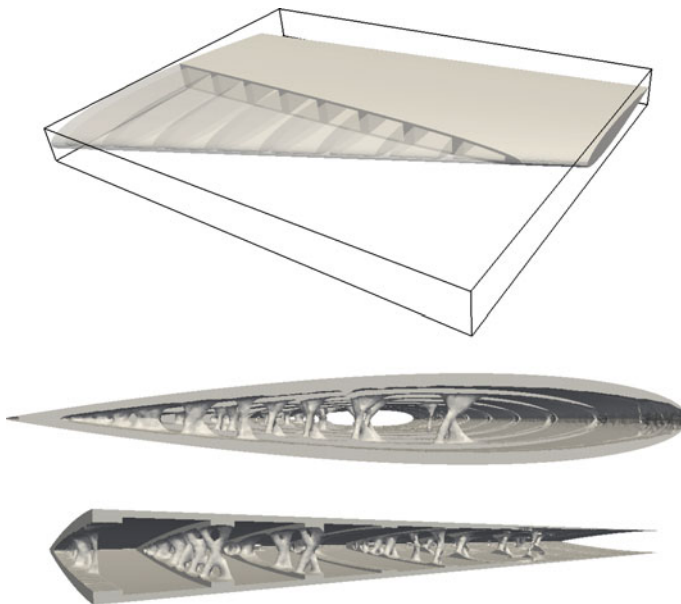


**Fig. 14.4** Topological optimization with an interior rib structure. Initial iteration (top) and two different cuts through the optimal solution (middle and bottom)

### 14.3 Optimization of the Distribution of Orthotropic Composite Material in the Wing Shell

We model the material in the wing shell as an orthotropic material, where one material direction coincides with the normal vector in each point in the shell. The other two material direction are described by a rotational angle around the normal vector. Thus, we optimize the distribution of this orientation angle as a function  $\alpha : \Omega_1 \rightarrow \mathbb{R}$ . This function enters the material properties in the form  $C(\alpha) = T(\alpha)C_1T(\alpha)^T$ , where  $T(\alpha)$  denotes the transformation of the reference coordinates, which depends on the angle  $\alpha$ , and  $C_1$  denotes a fixed orthotropic reference material.

The methods are implemented within the software toolbox FEniCS already mentioned in Sect. 14.2. In a first approach, we applied gradient based methods to the problem of determining the orientation angle distribution  $\alpha$ , where the derivative information is produced via an adjoint solution and the optimization itself is performed by a limited memory quasi-Newton method. This approach is viable, although additional regularization techniques have to be applied, but in total it takes up very much computational time. However, in [9] P. Pederson has proposed an analytic approach in a rectangular 2D setting and derived necessary optimality conditions for this specific case. There, for certain materials, the stronger material direction coincides with the direction of maximal stress and strain. We use this characterization in the 3D case in the wing shell and implement it in the form of a fixed point iteration, where each iteration step consists of the following algorithm:

1. Solve the linear elasticity equation
2. Determine in each the eigenvector of the largest stress in each point and project it to the shell manifold
3. Set the orientation angle to the direction from step 2.

For the start, it has shown advantageous, to initialize the iterations at the orientation according to the maximal strain. The resulting overall method gives the same solution, however, in a much more efficient way. Investigations into the convergence properties are performed in [22]. In an additional step, we combine this algorithm with the topology optimization approach from Sect. 14.2. This combination is implemented in a simultaneous fashion, where after each topology optimization step a fast approximative solution of the orthotropic material optimization in the wing shell is carried out. The resulting method converges to a joint optimum (for the wing interior as well as for the wing shell). Figure 14.5 shows exemplaric results for the optimal fiber orientation in the wing shell for a wing with two interior ribs.

A detailed analysis of the spatial distribution of the optimal solution shows that it can be separated in two intertwined and smoothly varying scalar fields which lead to two perpendicular orientation angles in each point. Figure 14.6 shows an example of a solution of the coupled problem of topology orientation in the wing interior together with the fiber optimization of the wing shell.

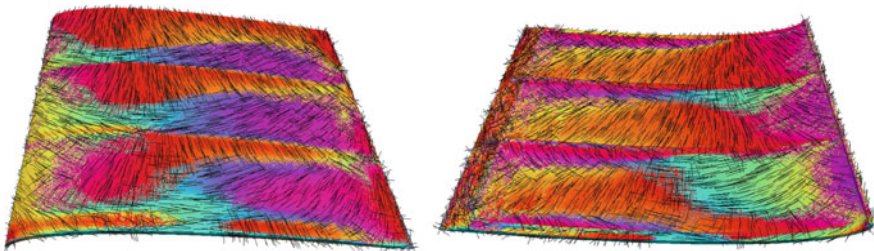


**Fig. 14.5** Optimized fiber orientations of a wing with two interior ribs (upper shell left, lower shell right)

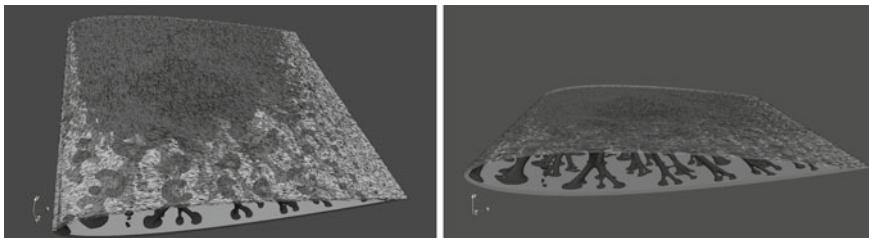


Fig. 14.6 Coupled optimal solution

### 14.4 Deformation Aspects, Multiple Load Case and Regularization

Wings with interior rib structures show characteristic bulges, when aerodynamic forces bend the whole wing. Those bulges are to be reduced by an appropriate orientation distribution of the orthotropic composite material. Thus, a multicriteria optimization problem arises with the two goals global compliance reduction and local reduction of the bulges. Here, we use again the wing shown in Fig. 14.5 with rib structures as illustrated in Fig. 14.7.

On this wing, the following boundary value problem is solved:

$$\begin{aligned}
 -\operatorname{div}(\sigma(u)) &= 0 \text{ in } \Omega \\
 \sigma(u) &= C(\alpha)\varepsilon(u) \text{ in } \Omega \\
 u &= 0 \text{ on } \Gamma_D \\
 \sigma(u)n &= 0 \text{ on } \Gamma_{\text{tip}} \\
 \sigma(u)n &= pn \text{ on } \Gamma_N
 \end{aligned}$$

where  $p$  denotes the aerodynamic pressure. The resulting bended wing is shown in Fig. 14.8, where the bulges are scaled in order to illustrate the investigated effects.

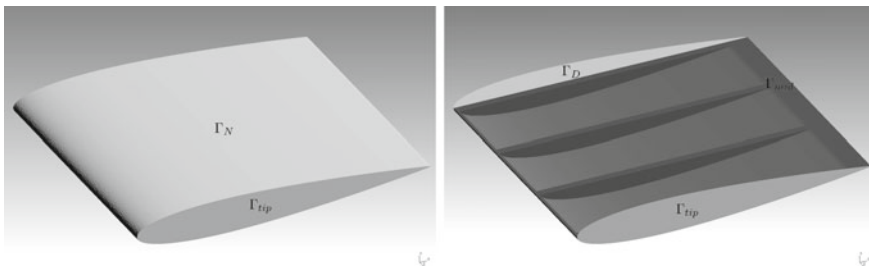
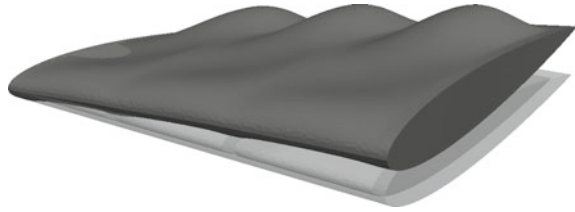
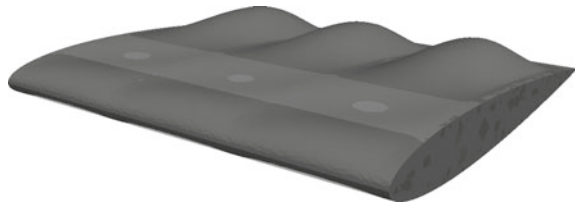


Fig. 14.7 Wing with rib structure as used in the numerical computations

**Fig. 14.8** Wing bending with scaled bulges



**Fig. 14.9** Pure bulge deformation of the wing ( $b$ , scaled)



The deformation  $u : \Omega \rightarrow \mathbb{R}^3$  is compared with a resulting deformation  $v : \Omega \rightarrow \mathbb{R}^3$  which bends the wing in the same way (prescribed by Dirichlet condition on the interior plane) but without the action of aerodynamic forces, i.e., as the solution of the boundary value problem

$$\begin{aligned}
 -\operatorname{div}(\sigma(v)) &= 0 \text{ in } \Omega \\
 \sigma(v) &= C(\alpha)\varepsilon(v) \text{ in } \Omega \\
 v &= u \text{ on } \Gamma_{\text{tip}} \cup \Gamma_{\text{mid}} \\
 v &= 0 \text{ on } \Gamma_D \\
 \sigma(u)n &= 0 \text{ on } \Gamma_N
 \end{aligned}$$

From this result, we compute the pure bulge deformation as  $b := u - v : \Omega \rightarrow \mathbb{R}^3$  without a global deformation of the wing, as shown in Fig. 14.9.

The vector field  $w := v + \lambda b$  ( $\lambda \in \mathbb{R}$ ) corresponds to a deformation of the wing with scaled bulges (scaling factor  $\lambda = 50$  in Fig. 14.8). The optimal fiber orientation according to the algorithm sketched above and with usage of  $w$  instead of  $u$  leads to the effect that the bulges are reduced, if the scaling factor  $\lambda$  is increased—sacrificing compliance to some extent. It should be noted that the overall algorithmic effort is only increased by a factor of 2: two elasticity problem are to be solved in each iteration ( $u$  and  $v$ ), but the optimization algorithm yields the same performance. The resulting Pareto diagram is shown in Fig. 14.10.

Figure 14.11 shows two optimized fiber orientation distributions, where the color code matches the one in Fig. 14.5.

In order to achieve results which are robust under uncertainties with respect to the specific aerodynamic forces, we consider furthermore the multiple load case. It is obvious that the algorithmic approach discussed above of guiding the fiber orientation with the direction of maximal stress cannot be carried over to this problem



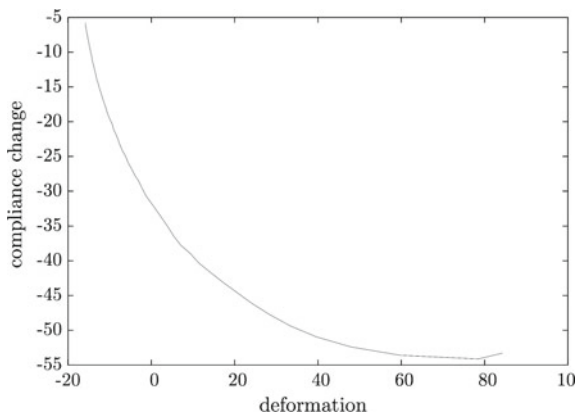


**Fig. 14.10** Pareto front of compliance reduction versus bulge reduction ( $0 \leq \lambda \leq 60$ ), shown are percentage values of the difference in comparison to the reference solution with overall constant fiber orientation

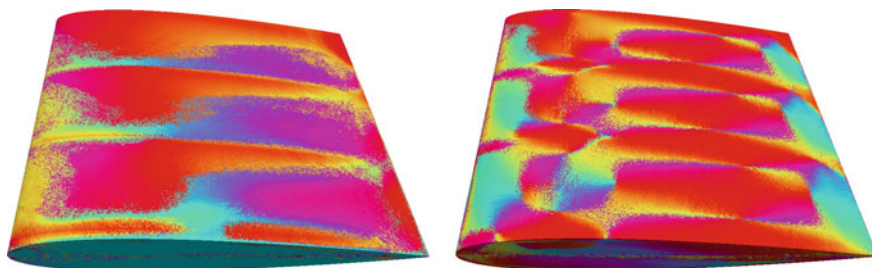


**Fig. 14.11** Two optimal fiber orientation distributions: left  $\lambda = 1$ , right  $\lambda = 40$

formulation. Here, we develop the following different approach which is computationally more expensive but can be generalized to the multiple load case. It is related to the methods discussed in [23] for the 2D case only. We represent the compliance as a trigonometric polynomial in the form

$$W_{\Omega} = \int_{\Omega} W(\alpha) dx = \int_{\Omega} a_0 + a_1 \sin(2\alpha) + b_1 \cos(2\alpha) + a_2 \sin(4\alpha) + b_2 \cos(4\alpha) dx \tag{14.1}$$

where the coefficients  $a_0, a_1, b_1, a_2, b_2$  are scalar functions depending on the location  $x \in \Omega$  which are composed of the (constant) material tensor and the strains  $\sigma : \Omega \rightarrow \mathbb{R}^3$ . In the multiple load case (with index  $k$ ), we obtain with weights  $\gamma_k \geq 0$  the weighted sum of the load cases in complete analogy as

$$\sum_k \gamma_k W_\Omega^k = \int_\Omega \bar{a}_0 + \bar{a}_1 \sin(2\alpha) + \bar{b}_1 \cos(2\alpha) + \bar{a}_2 \sin(4\alpha) + \bar{b}_2 \cos(4\alpha) dx \quad (14.2)$$

where, e.g.,  $\bar{a}_1 := \sum_k \gamma_k a_1^k$ ,  $a_1^k$  being the coefficient of the load case  $k$ , and the other coefficients  $\bar{a}_0, \bar{b}_1, \bar{a}_2, \bar{b}_2$  are defined analogously. Thus, formally, there is almost no difference between the single load case and the multiple load case. As the necessary condition for optimality, the derivative of the integrand above has to vanish in each  $x \in \Omega$ . Thus, at most four roots of the (differentiated) trigonometric polynomial have to be computed efficiently by reformulation as a polynomial in the complex plane. The root with the smallest contribution in the objective gives the new fiber orientation. A detailed derivation can be found in [22]. In total, we obtain the following algorithm in each optimization iteration:

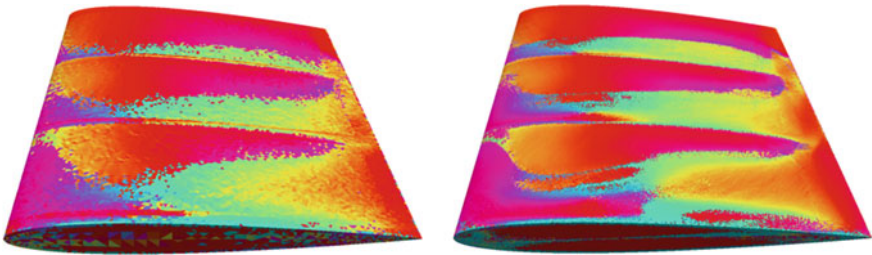
1. (parallel) computation of the linear elasticity equation for all load cases
2. (parallel) computation of the distributed coefficients  $\bar{a}_0, \bar{a}_1, \bar{b}_1, \bar{a}_2, \bar{b}_2$
3. solution of the local scalar optimization problems for the trigonometric polynomials in the FE grid
4. setting the fiber orientation to the direction from step 3.

In the single load case setting, the overall computational effort for this approach is between the effort for the method discussed in Sect. 14.2 and the approach via an adjoint solver discussed above. It increases linearly with the number of load cases. Furthermore, this approach gives good grid convergence as shown in Fig. 14.12, in all cases.

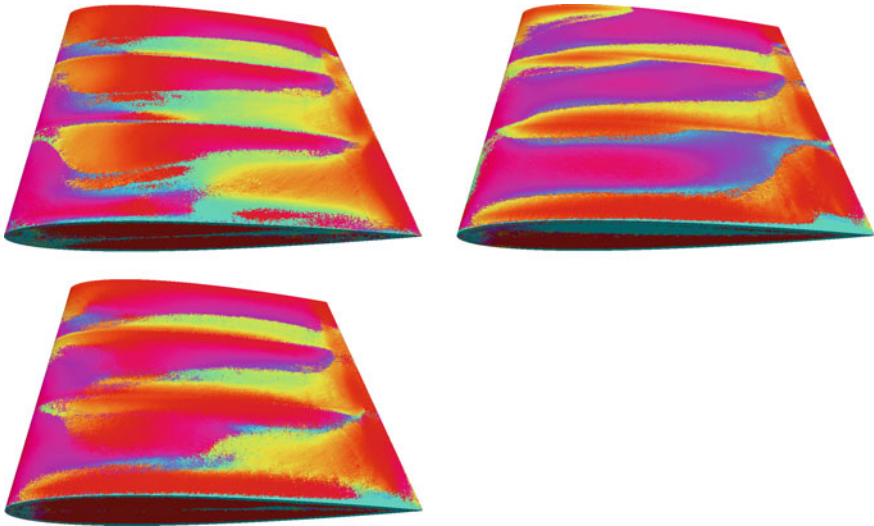
In Fig. 14.13, we show results for a multiple load scenario.

Figure 14.14 presents the convergence history for the multiload case. For each case (two single loads and one multiload case), we evaluate all three objectives. It can be observed in particular that the multiple load optimization yields a good compromise between the two separate objectives.

In the same way, as Eq. (14.1) is generalized to the multiple load case in Eq. (14.2), it can also be generalized to the incorporation of a regularization. We denote by  $\bar{\alpha} : \Omega_1 \rightarrow \mathbb{R}$  an orientation distribution of which we plan stay in a vicinity. Since the effect of the orientation is periodic in  $\pi$ , this periodicity has to be reflected also



**Fig. 14.12** Grid convergence in single load case: left coarse grid, right fine grid



**Fig. 14.13** Multiple load results: top row shows optimal solutions in two load cases, bottom shows the optimal solution in the equally weighted load case ( $\gamma_1 = \frac{1}{2} = \gamma_2$ )

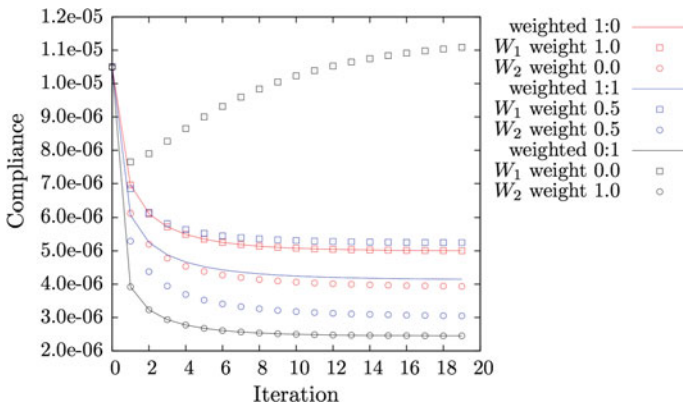


**Fig. 14.14** Convergence histories in the multiple load case study

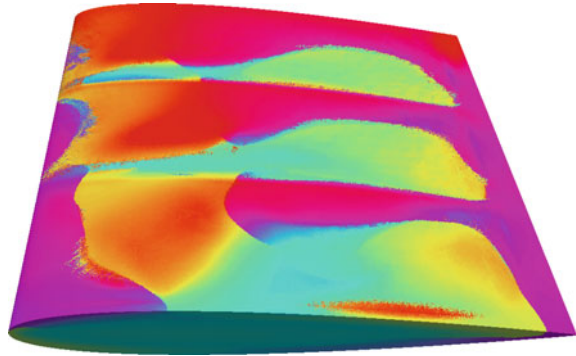
in the regularization term. In a regularized optimization, we use the objective

$$W_{\Omega}^{pen} := W_{\Omega} + \mu R(\alpha, \bar{\alpha}), \quad \mu > 0$$

where  $R(\alpha, \bar{\alpha})$  is defined by

$$R(\alpha, \bar{\alpha}) = \int_{\Omega} \cos\left(-\frac{\pi}{2} - 2\bar{\alpha}\right) \sin(2\alpha) + \sin\left(-\frac{\pi}{2} - 2\bar{\alpha}\right) \cos(2\alpha) + 1 dx$$

**Fig. 14.15** Regularized result



Thus,  $R(\alpha, \bar{\alpha})$  periodically penalizes deviations of  $\alpha$  from  $\bar{\alpha}$ , where deviations by  $\pi/2$  are penalized most. As a result, the coefficients of the trigonometric polynomial in Eq. (14.1) have to increased as

$$a_0^{pen} := a_0 + \mu, \quad a_1^{pen} := a_1 + \mu \cos\left(-\frac{\pi}{2} - 2\bar{\alpha}\right), \quad b_1^{pen} := a_1 + \mu \sin\left(-\frac{\pi}{2} - 2\bar{\alpha}\right)$$

and analogously in the multiple load case. Figure 14.15 shows a regularized single load case solution on a fine grid, where the regularizing angle distribution  $\bar{\alpha}$  has been generated by smoothing an unregularized result with the usage of the Laplace-Beltrami operator. Much clearer separations between the regions of different orientation angles are visible. In the smoothed result, the compliance is deteriorated by roughly 3% only.

## 14.5 Conclusions

We have developed methods for the topology optimization of aircraft wings, as well as methods for the optimal orientation of orthotropic composite material in the wing shell. Furthermore, practical aspects as reduction of buckling, the multiple load case and regularization have been considered. The numerical results are based on a linear elasticity model for the mechanical behavior of the wing. All implementations have been performed on the basis of FEniCS [21]. The results show a significant performance potential of alternative wing shapes and configurations.

## References

1. M. Stingl, M. Kočvara, G. Leugering, A sequential convex semidefinite programming algorithm with an application to multiple-load free material optimization. *SIAM J. Optim.* **20**, 130–155 (2009)
2. S. Osher, R. Fedkiew, *Level Set Methods and Dynamic Implicit Surfaces* (Springer, New York, 2003)
3. S. Schmidt, V. Schulz, A 2589 line topology optimization code written for the graphics card. *Comput. Vis. Science* **14**, 249–256 (2011)
4. M.P. Bendsøe, O. Sigmund, *Topology Optimization: Theory, Methods and Applications* (Springer, Berlin, 2003)
5. S. Schmidt, V. Schulz, Shape derivatives for general objective functions and the incompressible Navier-Stokes equations. *Control Cybern.* **39**, 677–713 (2010)
6. M.C. Delfour, J.-P. Zolesio, *Shapes and Geometries Analysis, Differential Calculus, and Optimization* (SIAM, 2001)
7. J. Sokolowski, A. Zochowski, On the topological derivative in shape optimization. *SIAM J. Control Optim.* **37**, 1251–1272 (1999)
8. B. Mohammadi, O. Pironneau, *Applied Shape Optimization for Fluids* (Oxford University Press, New York, 2001)
9. P. Pedersen, On optimal orientation of orthotropic materials. *Struct. Optim.* **1**, 101–106 (1989)
10. S. Schmidt, C. Ilic, N. Gauger, V. Schulz, Airfoil design for compressible inviscid flow based on shape calculus. *Optim. Eng.* **12**, 349–369 (2011)
11. S. Schmidt, C. Ilic, N. Gauger, V. Schulz, Three dimensional large scale aerodynamic shape optimization based on shape calculus, in *41st AIAA Fluid Dynamics Conference and Exhibit, AIAA 2011–3718* 2011
12. G. Allaire, F. Jouve, A.M. Toader, Structural optimization using sensitivity analysis and a level-set method. *J. Comput. Phys.* **194**, 363–393 (2004)
13. J.A. Sethian, *Level Set Methods and Fast Marching Methods* (Cambridge University Press, Cambridge, 1999)
14. A.A. Novotny, R. Feijoo, E. Taroco, C. Padra (1992), Topological sensitivity analysis for three-dimensional linear elasticity problem, in *6th World Congress on Structural and Multi-disciplinary Optimization Rio de Janeiro, 30 May–03 June 2005* (Brazil, 2005)
15. R. Stoffel, Structural Optimization of Coupled Problems, Dissertation, Universität Trier, 2013
16. S. Amstutz, H. Andrä, A new algorithm for topology optimization using a level-set method. *J. Comput. Phys.* **216**, 573–588 (2006)
17. S. Giusti, A.A. Novotny, C. Padra, Topological sensitivity analysis of inclusion in two-dimensional linear elasticity. *Eng. Anal. with Bound. Elem.* **32**, 926–935 (2008)
18. S. Amstutz, Sensitivity analysis with respect to a local perturbation of the material property. *Asymptot. Anal.* **49**, 87–108 (2006)
19. S. Amstutz, A.A. Novotny, E. de Suza Neto, Topological derivative-based topology optimization of structures subject to drucker-prager stress constraints. *Comput. Methods Appl. Mech. Eng.* **233–236**, 123–136 (2012)
20. D.E. Campeao, A.A. Novotny, Topological derivative-based structural optimization considering different volume control methods. Technical report, Coordenacao de Matematica Aplicada e Computacional, Laboratorio Nacional de Computacao Cientica LNCC/MCT (Petropolis, Brazil, 2011)
21. A. Logg, K.-A. Mardal, G.N. Wells et al., *Automated Solution of Differential Equations by the Finite Element Method* (Springer, Berlin, 2012)
22. H. Zorn, Optimierung der Materialausrichtung von orthotropen Materialien in Schalenkonstruktionen, Dissertation, Universität Trier, 2017
23. H.C. Cheng, N. Kikuchi, Z.D. Ma, An improved approach for determining the optimal orientation of orthotropic material. *Struct. Optim.* **8**, 101–112 (1994)
24. J. Sokolowski, J.-P. Zolesio, *Introduction to Shape Optimization* (Springer, Berlin, 1991)